World Electric Vehicle Journal

MDPI

Article

Comparative Concept Study of Passive Hybrid Energy Storage Systems in 48 V Mild Hybrid Vehicles Varying Lithium-Ion Battery and Supercapacitor Technologies †

Thorsten Grün * and Martin Doppelbauer

Karlsruhe Institute of Technology (KIT), Institute of Electrical Engineering (ETI), Hermann-von-Helmholtz-Platz 1, 76344 Eggenstein-Leopoldshafen, Germany; martin.doppelbauer@kit.edu

* Correspondence: thorsten.gruen@kit.edu; Tel.: +49-721-608-28282

† This paper is an extended version of a paper presented at 32nd International Electric Vehicle Symposium 2019 (EVS 32), Lyon, France, 19–22 May 2019.

Received: 10 October 2019; Accepted: 29 October 2019; Published: 1 November 2019

Abstract: A single energy storage technology will deliver either high power or high energy density. In high cycle applications like 48 V mild hybrid electric vehicles, lithium-ion batteries or supercapacitors have to be oversized to meet power, energy and cycle life requirements. However, a passive hybrid energy storage system is able to meet those challenges, but its performance depends on several factors. In this study, simulations and experimental investigations show how the design and operation conditions influence the performance of a passive hybridized system. In a comparative study for 48 V systems, consequences on performance are discussed.

Keywords: hybrid electric vehicles (HEV); lithium-ion battery; supercapacitor; modeling; regenerative braking

1. Introduction

Considering the requirements of an energy storage system (ESS) for current generations of 48 V mild hybrid electric vehicle (MHEV) (Gen1: 11 kW; ~320 Wh) [1], a high power to energy (P/E) ratio and a high cycle lifetime is mandatory. Future generations (Gen3: 25 kW; 1–5 kWh) of MHEVs will require a different P/E ratio in order to enable pure electric driving within cities (FHEV = full hybrid electric vehicle) [2]. Lithium-ion batteries (LIB) in form of high-energy (HE) or high-power (HP) cells and even supercapacitors (SC) as a single system cannot satisfy all requirements in terms of P/E ratio and cycle life without oversizing and/or overstraining the system. Therefore, a hybrid energy storage system (HESS) and specifically a passive HESS is a suitable approach for pulse load profiles, which appear in MHEVs and even in FHEVs.

Passive HESS show higher efficiencies and less complexity than other HESS solutions [3]. However, their performance is mainly determined by the technology matching in terms of voltage characteristics and ohmic resistance ratio whereas new degrees of freedom arise on system level. Different LIB technologies and even more so conventional electrochemical double layer capacitors (EDLC) exhibit quite different characteristics in ohmic resistances and voltages. New capacitor technologies like Lithium-carbon capacitors (LIC) [4–6] arise that fill the gap in power and energy density between LIB and SC technologies and bring new flexibilities in the design of passive HESS.

This study shows by experimental and model-based investigations how the design of a passive HESS and its operation condition influence power and energy density. Advantages over battery-only ESSs are discussed in a comparative study by analyzing two virtual 48 V MHEV scenarios.

2. Fundamentals

2.1. Pulse Current Load and Operating Voltage

Factors that have an impact on the performance of a HESS within pulse load profiles have already been discussed in previous papers. Besides the setup and the capacity ratio of the LIB or the SC [6,7], also the characteristic of the pulse load profile and its impact were part of the discussion [8,9].

The character of a pulse load profile can be described by its period (T) and the pulse duration (PD), in which the load current (I_{load}) is active. In Figure 1a a given current versus time I_{load} (t) is presented schematically for two different periods (T_1 and T_2) as well as for two different pulse durations (PD_1 and PD_2). Using Equation (1) the pulse profile can be characterized by its duty cycle (D), which describes the relationship between the period T and the pulse duration PD.

$$D = \frac{PD}{T} \tag{1}$$

The individual voltage limits of two hybridized energy storage technologies determine the permissible voltage operating range. The upper cut-off voltage (U_{max}) or the lower cut-off voltage (U_{min}), whichever is violated first, determines the actual operating range of the HESS. The usable energy of a HESS ($E_{HESS,\ total}$) is limited to the difference of the available capacities Q_1 and Q_2, which depend on the upper (U_{max}) and lower cut-off voltage (U_{min}) of the HESS (see Figure 1b).

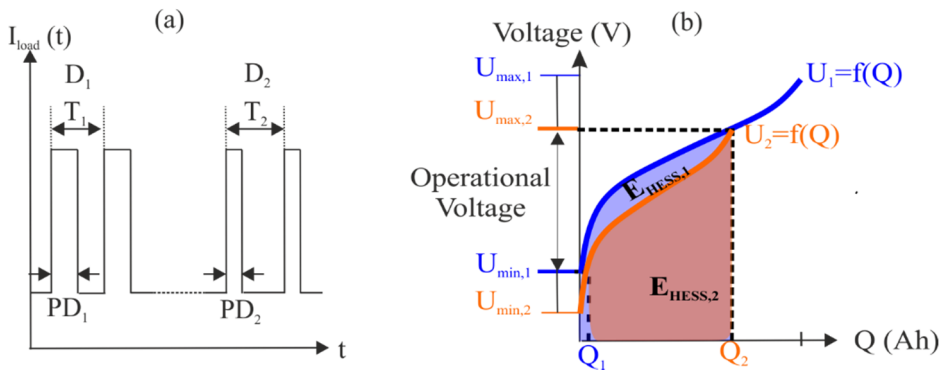

Figure 1. (**a**) Schematic of pulse load profile with two different characteristics in pulse duration (PD) and period T resulting in two different duty cycles D; (**b**) representation of upper and lower cut-off voltages (U_{max} and U_{min}) on the operating voltage range of a passive hybrid energy storage system (HESS) and usable energy of each component.

The usable energy of a HESS $E_{HESS,total}$ is the sum of the usable energies of each energy storage $E_{HESS,1}$ and $E_{HESS,2}$, which can be calculated by the integration of the voltage curve U_1 and U_2 by the capacity within the limits Q_1 and Q_2 (see Equation (2)).

$$E_{HESS,total} = \int_{Q_1}^{Q_2} U_1(Q)dQ + \int_{Q_1}^{Q_2} U_2(Q)dQ \tag{2}$$

2.2. Characterization of Energy Storage System (ESS) during Pulse Load Profiles

Energy and power density are typical dimensions to describe the characteristics of an ESS. The energy density (e_{ESS}) defines which energy can be extracted per mass (m_{ESS}) of the ESS. In [10], it is proposed to integrate time-varying voltage U (t) and load current I_{load} (t) only during active pulses (g = 1) and to neglect U (t) and I_{load} (t) during pulse off times (g = 0). To characterize the power density p_{ESS}, e_{ESS} is divided by the product of total time τ and κ, whereby κ is the fraction of τ in which

the current pulse is active. The energy density e_{ESS} and the power density p_{ESS} can be calculated by Equations (3) and (4):

$$e_{ESS} = \frac{1}{m_{ESS}} \int_0^{\tau} U(t) \cdot I_{load}(t) \cdot g(t) dt \tag{3}$$

$$p_{ESS} = \frac{e_{ESS}}{\tau \kappa} \tag{4}$$

The P/E ratio is given in (1 h^{-1}) and describes the ratio between power and energy density of an ESS and it is also used to specify the requirements of P/E ratio for applications. Depending on the degree of electrification of an xHEV, the P/E Ratio can hold a value of 3 h^{-1} until 40 h^{-1} [11].

3. Modeling

It is one objective of this study to derive a universal cell model (CM) for a variety of LIB and SC technologies along with a standardized parameter determination, which simplifies the design processes for HESSs. Besides commercial LIBs, such as lithium-ion phosphate (LFP) and lithium-ion cobalt oxide (LCO), conventional EDLC technologies, and two different types of LIC technologies are also investigated in this study.

There are two general concepts that use both LIB and SC materials for the electrodes, either as a serial or parallel connection. The composition of the electrodes differs between the two concepts. In serial connection, one electrode consists of battery material and the other one holds EDLC material and forms a serial hybrid capacitor (SHC). A parallel hybrid capacitor (PHC) consists of so-called bi-material electrodes which are containing EDLC and battery material [12].

3.1. Cell Model (CM)

The Thevenin model is used as the cell model which is a common method to describe the electrical behavior of LIBs [13,14]. Considering state of the art modeling of EDLCs, the Thevenin model is similar to the "classical model" for EDLCs [15] but extended by a voltage source.

The model consists of a voltage source to represent the open circuit voltage (U_{ocv}), the ohmic resistance (R_{inter}) which describes the ohmic losses due to electrolyte and electrodes and one RC-circuit (with R_{RC} and C_{RC}) to take diffusion processes within electrochemical energy storage devices into account. The terminal voltage (U_{cell}) can be calculated by Equation (5), considering the dynamics of U_{RC} between two-time samples (Δt) in Equation (6).

$$U_{cell}(t) = U_{OCV}(t) + I(t) \cdot R_{inter}(t) + U_{RC}(t) \tag{5}$$

$$U_{RC}(t) = U_{RC}(t-1) e^{\frac{-\Delta t}{R_{RC}(t) C_{RC}(t)}} + \left(1 - e^{\frac{-\Delta t}{R_{RC}(t) C_{RC}(t)}}\right) R_{RC} \cdot I(t-1) \tag{6}$$

3.2. Single Cell Characteristics and Parameter Determination

R_{inter} is determined by the R_{DC} pulse method [16] in which the pulse duration PD is varied depending on the cell technology. Using Ohm's law, R_{inter} can be calculated from the resulting change in voltage caused by the applied current. This procedure is performed for a state of charge (SOC) of 10% to 90% in 10% steps in discharge (DIS) direction and will be used as a look-up table within the simulation tool. For LIBs, the pulse is performed for 20 s and for all SC technologies, R_{inter} given in the datasheets are reached by a 2 s pulse.

The parameterization procedure of U_{OCV} is slightly different between cell technologies. For LIB and LIC_{PHC}, U_{OCV} is measured in a 2.5% SOC interval starting from 100% SOC and a relaxation time of 20 min, after each point interval is reached. In case of EDLC and LIC_{SHC}, U_{OCV} is measured by a continuous 1 C charge starting at U_{min} until U_{max}. Measured parameters for modeling U_{OCV} and R_{inter} characteristics are given in Figure 2. R_{RC} and C_{RC} are determined by using Matlab® Optimization Toolbox (The MathWorks, Inc., Natick, MA, USA) in which a nonlinear Levenberg–Marquardt algorithm

is used to fit the parameters R_{RC} and C_{RC} in the least square sense to minimize modeled and measured error of U_{cell}.

Besides the high-energy versions of LIBs (LFP_{HE} and LCO), also a high-power oriented LFP cell (LFP_{HP}) is parameterized for the virtual concept study. To analyze energy and power density, each cell is charged by a 1 C constant-current–constant-voltage (CCCV) regime until the upper cut-off voltage U_{max} and a cut-off current of C/20 are reached. Afterwards, each cell is discharged with a pulse load profile with a duty cycle D of 0.5 at pulse duration PD set to 10 s until the lower cut-off voltage U_{min} is reached. In general, power densities consider mainly maximum allowed C-Rates in DIS direction, which for most LIBs are higher than in charge (CHG) direction. One of the most crucial design constraints in ESS design of MHEVs are the high peak currents in CHG direction (~230 A for 11 kW at 48 V). Hence, for power and energy density measurement, the highest allowed C-Rates for CHG direction are applied. The experiments are performed at room temperature (approximately 25 °C), but due to the applied load, cells heated up. The maximum cell temperature has been achieved by LIC_{PHC} with approximately 36.6 °C at 150 A. The maximum temperatures for the other cells have been in a range between 25.2 °C and 33.6 °C. Measured energy and power density for all cells under study are presented in Table 1 along with further technical data.

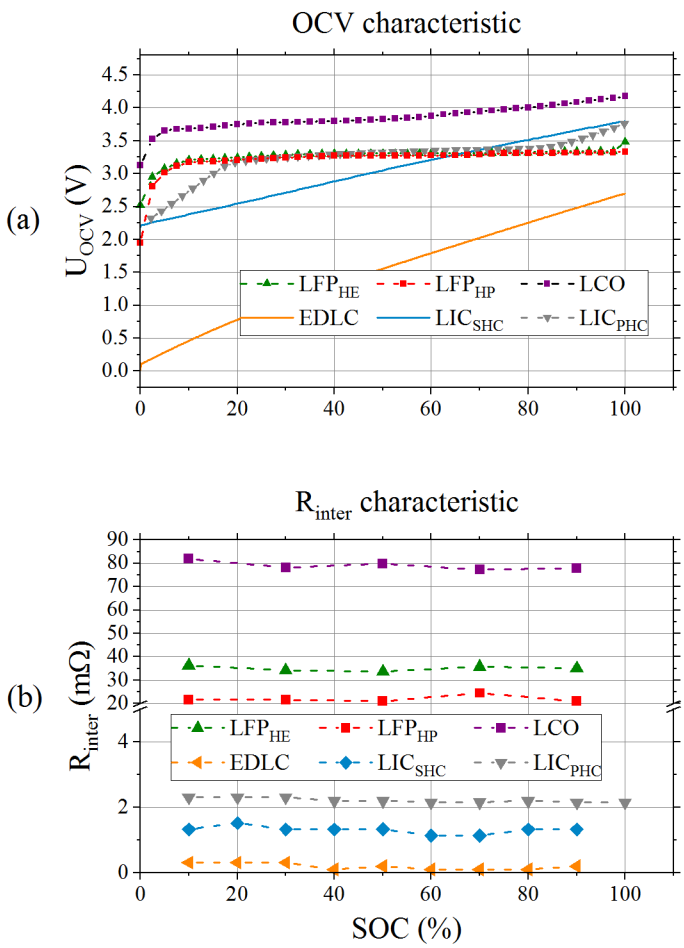

Figure 2. Measured parameter for cells under study; (**a**) measured open circuit voltage (OCV) characteristics for lithium-ion batteries (LIB) and supercapacitors (SC); (**b**) R_{inter} characteristics for OCV and SC technology with R_{DC} pulse measurement.

Table 1. Technical data of cells under study including measured energy/power densities and capacities.

Cell Type	Cell Design	Capacity (Ah)	Voltage Range (V)	Mass (kg)	Volume (l)	C-Rate Max CHG	e_{ESS} ($Whkg^{-1}$)	p_{ESS} (Wkg^{-1})
LCO	18650	2.45	2.5–4.2	0.045	0.017	0.75	209.45	149.71
LFP_{HE}	26650	3.00	2.0–3.6	0.085	0.036	1	109.54	109.89
LIC_{SHC}	Pouch	1.28	2.2–3.8	0.250	0.150	117	11.29	1722.96
LIC_{PHC}	Pouch	4.30	2.2–3.8	0.270	0.150	35	35.14	1555.65
EDLC	Cylindrical	2.25	0.1–2.7	0.540	0.390	471	5.88	745.43 *
LFP_{HP}	26650	2.50	2.0–3.6	0.076	0.036	4	101.14	411.98

* Maximum allowed C-Rate could not be supplied due to test bench limitation (max 200 A). A higher p_{ESS} is possible.

3.3. From Cell Model (CM) to System Model (SM)

In a battery pack many cells are connected in a hierarchal manner by serial and/or parallel connection (xSyP) to meet the voltage, power and/or energy requirements of the application. To derive a system model (SM) from a cell model, the parameters of the cell model are scaled up according to the configuration (xSyP) to emulate the time dependent voltage and resistance characteristics of the system (see Equation (7)). The indices (LIB, SC) imply the considered technology. This method is quite accurate as long as no intrinsic cell imbalances are assumed [17]. Calmer's rule is applied to solve Equation (7) for I_{LIB}, and according to Kirchhoff's current law, the current of the SC bank I_{SC} can be calculated from the difference between I_{LIB} and I_{load} given in Equation (8).

$$\begin{bmatrix} 1 & 0 \\ \left(-R_{inter,SC}(t)\cdot\frac{S_{SC}}{P_{SC}}\right) & \left[\left(R_{inter,SC}(t)\cdot\frac{S_{SC}}{P_{SC}}\right)+\left(R_{inter,LIB}(t)\cdot\frac{S_{LIB}}{P_{LIB}}\right)\right] \end{bmatrix}\begin{pmatrix} I_{load}(t) \\ I_{LIB}(t) \end{pmatrix} = \begin{pmatrix} I_{load}(t) \\ \left(U_{OCV,LIB}(t)+U_{RC,LIB}(t)\right)S_{LIB}-\left(U_{OCV,SC}(t)+U_{RC,SC}(t)\right)S_{SC} \end{pmatrix} \tag{7}$$

$$I_{SC}(t) = I_{load}(t) - I_{LIB}(t) \tag{8}$$

As the currents in Equations (7) and (8) are calculated on the system level, the changing SOC must be considered within the cell model. The SOC is calculated by Equation (9) in which the integral of the current I is divided by the product of the nominal capacity (C_N) and the number of cells P that are connected in parallel.

$$SOC(t) = \frac{1}{P\cdot C_N}\int_{t=0}^{t} I dt \cdot 100\% \tag{9}$$

An overview of the algorithm containing upscaling the cell model parameters of the used electrical circuit model (ECM) in Figure 3a along with the calculation of load distribution and a drawback to parameter dynamics is given in Figure 3b.

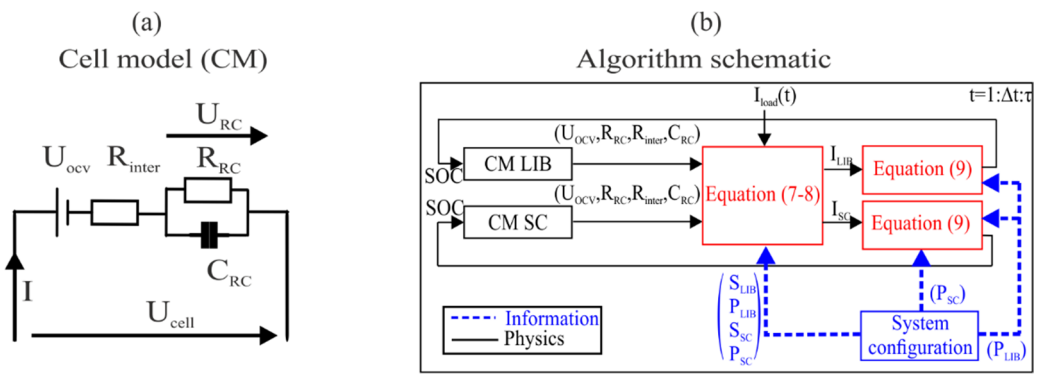

Figure 3. Schematics of the cell model (**a**) and the algorithm for system modeling (**b**).

4. Analysis

The analysis of passive HESS is conducted by experimental and model-based approaches. Within experimental investigations, LIB and SC technologies are hybridized on cell level (C2C) and a 48 V system level (S2S). In focus are the energy and power density depending on technology matching, the system layout, and the impact of pulse load characteristics. To derive further findings of practical applicability of HESS, model-based analysis of nowadays (Gen1) and future-oriented (Gen3) MHEV applications are conducted.

4.1. Experimental Study of Energy Density and Power Density Enhancement

The determination of energy and power density of HESSs on C2C and S2S level is conducted in the same way as for the single cells (PD: 10 s; D: 0.5). Besides that, for S2S study, pulse duration PD and duty cycle D are changed according to the pulse duration and the duty cycle occurrence in application-oriented load profiles. For evaluating power density, only results, in which I_{LIB} is not exceeding its maximum allowed C-Rate counterpart, are taken into account. For the calculation of energy and power density Equations (3) and (4) are applied, whereas for S2S analysis only the cumulated mass of the used cells is considered to calculate m_{ESS}.

4.1.1. Cell to Cell Analysis (C2C)

A Basytec HPS Battery Tester (BaSyTec GmbH, Asselfingen, Germany) is used for the C2C experiments to provide I_{load} (PD: 10 s; D: 0.5) and to measure the terminal voltage of the HESS U_{HESS}. An Agilent Keysight 3872A (Agilent Technologies, Inc., Santa Clara, CA, USA) measures the voltage drop over a shunt resistance (1 mΩ) to identify I_{LIB} and I_{SC}. With Ohm´s law, I_{LIB} can be determined directly. Using Equation (8), I_{SC} can be calculated by using measurement data of I_{LIB} and I_{load} with a time resolution of 1 s. As HESS, LFP_{HE} and LCO are connected to all SC technologies under study. In the case of the EDLC, two EDLC have to be connected in serial to gain the voltage ranges of LIBs. The schematics of the test bench and data acquisition are presented in Figure 4a.

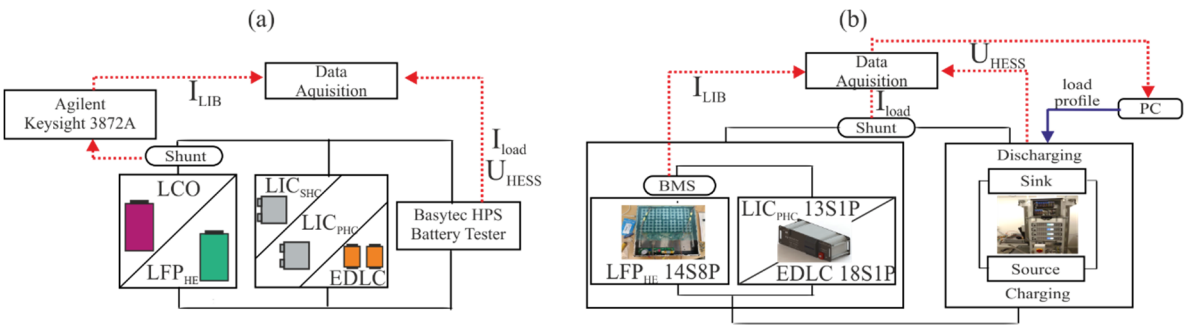

Figure 4. (**a**) Setup and schematic of cell to cell analysis (C2C) campaign with data acquisition; (**b**) setup and schematic of system to system analysis (S2S) campaign using energy storage system (ESS) of Table 2.

4.1.2. System to System Analysis (S2S)

For investigations on a S2S level, sinks and loads are used (cumulated max. 120 A CHG/DIS), whose load profiles can be controlled by a PC. The test bench principle is presented in Figure 4b and as for the C2C investigation, a shunt resistance (1 mΩ) is used to determine I_{load} in a time resolution of 0.2 s. In comparison to the C2C level, a battery management system (BMS) is necessary to satisfy safety requirements of the used 48 V ESS, which is also providing data like I_{LIB} for the evaluation and calculating I_{SC} according to Equation (7).

In application-oriented profiles, like HEV life cycle test in Figure 5a, a variety of pulse durations and duty cycles can be found. Therefore, conspicuous peak powers, like 11 kW peak power, are investigated

in terms of its pulse duration and duty cycle. For 11 kW peaks, an average pulse duration of 2 s at an average duty cycle of 0.03 occurs. Besides 2 and 10 s pulse durations, also 5 s is as pulse duration considered, hence following instructions of [1], ESS for MHEV applications should enable maximum power for 5 s.

The 48 V systems of LFP_{HE} and LIC_{PHC} are built as prototypes. For the 48 V EDLC system, a commercially available product is used. Energy and power densities are identified by the abovementioned regime and are presented in Table 2 along with measured capacities for a 1 A DIS after a 1 C CCCV CHG regime. Data acquisition, control, and analysis are accomplished using LabVIEW® (National Instruments Corporation, Austin, TX, USA). Four HEA-PSI91000-030U3 (HEIDEN electronics GmbH, Pürgen, Germany) are used as sink and four HEA-ELR91500-030 (HEIDEN electronics GmbH, Pürgen, Germany) are used as load. Data acquisition hardware components include one Q.gat_IP controller (Gantner Instruments Test & Measurement GmbH, Darmstadt, Germany), Q.bloxx_A107 (Gantner Instruments Test & Measurement GmbH, Darmstadt, Germany) with four universal analog input channels, and Q.bloxx_A127 (Gantner Instruments Test & Measurement GmbH, Darmstadt, Germany) with four voltage input channels.

Table 2. Technical data of 48 V energy storage system (ESS) under study.

System/Parameter	Topology	Voltage Range (V)	Capacity (Ah)	e_{ESS} (Whkg^{-1})	p_{ESS} (Wkg^{-1})
LFP_{HE}	14S8P	32.0–48.5	22.45	103.08	99.67
LIC_{PHC}	13S1P	30.7–47.5	3.46	21.69	1328.20 *
EDLC	18S1P	0.1–48	2.22	1.47	538.55 *

* Maximum current could not be supplied due to test bench limitation (max 120 A). A higher p_{ESS} is possible.

4.2. Model Validation and Virtual Concept Study

4.2.1. Model Validation

The model is validated by using the normalized-root-mean-square error (NRMSE) method. Firstly, simulated and measured voltages U_{cell} of the cell model during dynamic load profiles are validated. Secondly, the model accuracy in terms of I_{LIB}, I_{SC} and terminal voltage U_{HESS} of each HESS within C2C campaign for a constant load followed by a pulse load profile is investigated. At last I_{LIB}, I_{SC} and the terminal voltage on S2S level U_{HESS} are also validated by experiments of the S2S campaign. Calculated errors of I_{LIB} and I_{SC} are normalized to the range of maximum measured current in CHG and DIS of each. Voltage errors are normalized to the arithmetic mean value of measured terminal voltages U_{HESS} or U_{cell} respectively. Finally, NRMSE of SC and LIB are summarized as overall model accuracy by calculating arithmetic mean errors of current and voltage for each validation campaign.

4.2.2. Virtual Concept Study for Two Mild Hybrid Electric Vehicle (MHEV) Scenarios (Gen1–Gen3)

In the virtual concept study, the performance of HESS and commercial ESS using high-power or high-energy should be compared within realistic scenarios. The first study shall represent nowadays requirements for MHEV ESS. These are start-stop, regenerative braking, and acceleration tasks. For this simulation, the load profile of Figure 5a from the United States Advanced Battery Consortium (USABC) is used. The second study represents future tasks of MHEV, which involve additionally pure electric inner city driving. Thus, the given acceleration (a) and velocity (v) profiles of the worldwide harmonised light vehicles test procedure (WLTP) are converted into a power profile (P_v) by Equation (10) and using parameters of Table 3.

Table 3. Parameters for load profile computation for Gen3 emulation.

Mass of Vehicle m_v (kg)	Gravitational Acceleration g (ms^{-2})	Rolling Resistance C_r (-)	Density of Air ρ_{air} (kgm^{-3})	Drag Coefficient C_d (-)	Cross-Sectional Area A_{front} (m^2)	ESS Max Chg/Dis Power (kW)
1615	9.81	0.01	1.22	0.30	2.30	25

The Energy Management System (EMS) controls how a MHEV splits the power supply to the combustion engine (CE) and/or the ESS (see Equation (11)). Thus, a first-order approach is assumed following the regime described in Table 4 to emulate P_{ESS} which is plotted along with v in Figure 5b. The input parameter I_{load} (t) of the model is computed by P_{ESS} (t)/48 V.

$$P_v = \left(m_v \cdot a + m_v \cdot g \cdot C_r + \frac{1}{2}\rho_{air} \cdot C_d \cdot A_{front} \cdot v^2\right)v \tag{10}$$

$$P_v = P_{CE} + P_{ESS} \tag{11}$$

Table 4. Energy Management System (EMS) for mild hybrid electric vehicle (MHEV) application of Gen 3.

Mode	Condition	Description
Inner City Driving	$v < 50\ kmh^{-1}$	P_v is powered by ESS
Engine Mode	$50\ kmh^{-1} < v < 70\ kmh^{-1}$	P_v is powered by ESS and CE Linear decrease of P_{ESS} at $50\ kmh^{-1}$ to 0 kW at $70\ kmh^{-1}$ is assumed
Freeway Mode	$v > 70\ kmh^{-1}$	P_v powered by CE
Regenerative Braking	$a < 0$	Until 25 kW ESS is getting charged

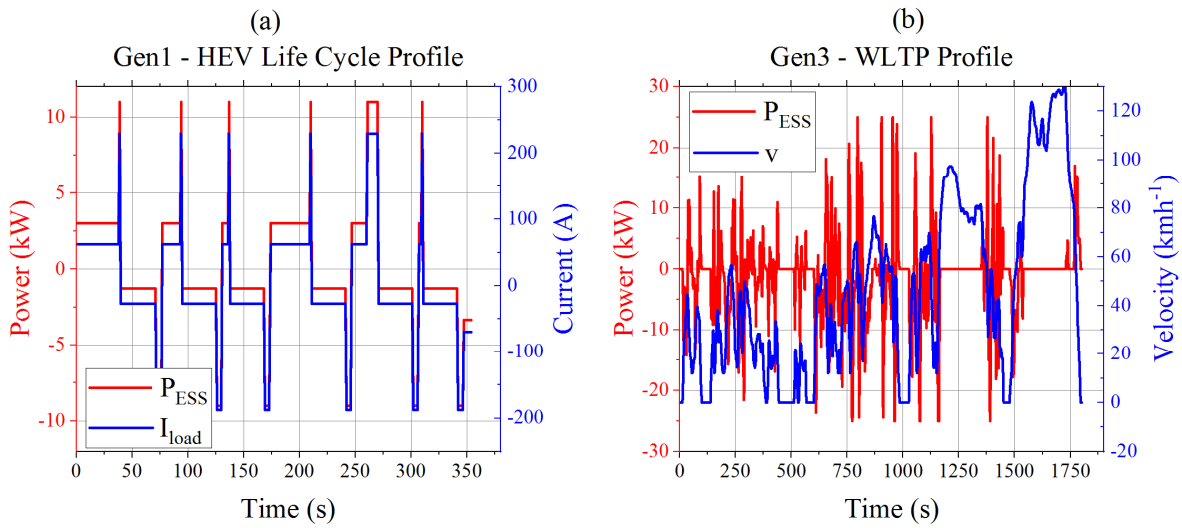

Figure 5. Profiles of virtual concept study; (**a**) power and current for hybrid electric vehicles (HEV) Life Cycle Profile proposed by United States Advanced Battery Consortium (USABC) for nowadays Gen1 mild hybrid electric vehicle (MHEV); (**b**) velocity profile of worldwide harmonised light vehicles test procedure (WLTP) and computed ESS power to emulate future Gen3 MHEV with inner-city driving mode.

The model-based investigation is divided into several studies, which are comparing weight and volume of a HESS and its competitive ESS as well as the charge throughput Q_{TP} and the root mean square of the current I_{RMS} of a single cell within a HESS and its competitive ESS.

As a unit for comparison the performance index (Θ) shall be introduced, which should emphasize the differences in dimensions (weight and volume) and also in terms of the stress of a LIB cell within both systems. Herein the relative deviation of the considered value of the hybrid system (X_{HESS}) to the value of the battery-only system (X_{ESS}) is calculated by Equation (12). Positive values of the performance index Θ emphasis advantages of the HESS over the ESS and negative values correspond to the contrary statement.

$$\Theta = \frac{(X_{ESS} - X_{HESS})}{X_{ESS}} \cdot 100\% \tag{12}$$

The number of serial cells is determined by the system voltage of 48 V whereas the number of parallel cells is dictated by the maximum C-Rate for each technology and the maximum peak of I_{load}. In general, those LIBs are not typical representatives of commonly used LIBs in automotive applications. However, the principal objective of this study is to determine if there are possible configurations of HESS with high energy cells that can compete with high power ESS. Another objective is to determine how existing ESS can be improved by a passive hybridization and which technology match suits best.

A number of virtual HESS and ESS are set up according to the following tables. Tables 5 and 6 are containing the setups of several HESS by using different supercapacitor technologies within the Gen1 and Gen3 scenarios for LCO and LFP_{HE} hybrid systems, which compete with battery-only systems ESS consisting of the same LIB equivalent technology. Two types of hybrid systems are set up which focus on design criteria like weight and volume. The index $HESS_{min}$ indicates hybrid systems, which are the lightest in their technology match whereas $HESS_v$ shall label systems, which have approximately the same volume as its battery-only counterpart. Table 7 contains setups of HESS systems for Gen1 and Gen3 scenarios, which are competing against energy storage systems setup of the presented LFP_{HP} high power cell.

Besides the analysis of operational behavior, it shall also be part of the discussion, whether the analyzed hybrid systems meet power to energy and energy density targets of Gen1 and Gen3 applications. Therefore, requirements in terms of weight, maximum power, and energy are summarized, and energy density, as well as P/E ratio, is calculated with respect to these values. Maximum weight and power for Gen1 applications are already given in [1]. As Gen3 applications are still in development and technical guidelines like for Gen1 are missing, maximum power value is taken from industry goals [2]. As 48 V MHEV for Gen3 applications should be able to fulfill tasks of nowadays FHEV applications, target values for the maximum weight are taken from USABC goals for HEV battery [11]. The energy consumption within inner city driving is for an electric car approximately 0.17 $kWhkm^{-1}$ [18], hence a range for the installed energy was chosen to allow driving distances within cities of 6 until approximately 30 km. Target specifications for Gen1 and Gen3 applications are listed in Table 8.

Table 5. Technical data of virtual LFP_{HE} (H)ESS concept study within Gen1 and Gen3 scenarios.

Characteristic/Profile	**Gen1–HEV**				**Gen3–WLTP**			
	EDLC	**LIC_{SHC}**	**LIC_{PHC}**	**ESS**	**EDLC**	**LIC_{SHC}**	**LIC_{PHC}**	**ESS**
LIB bank (xSyP) $HESS_{min}/HESS_{v}$	14S6P/14S67P	14S1P/14S69P	14S2P/14S69P	-/14S77P	14S39P/14S160P	14S37P/14S170P	14S34P/14S170P	-/14S174P
SC bank (xSyP) $HESS_{min}/HESS_{v}$	18S7P/18S1P	13S8P/13S2P	13S9P/13S2P	-	18S6P/18S1P	13S8P/13S1P	13S11P/13S1P	-
Weight (kg) $HESS_{min}/HESS_{v}$	75.18/89.45	27.19/88.61	33.97/89.13	-/91.62	104.73/200.12	70.03/205.55	79.07/205.81	-/207.05
Volume (l) $HESS_{min}/HESS_{v}$	52.16/40.78	16.29/38.72	18.77/38.72	-/38.80	61.77/87.66	34.34/87.65	38.84/87.65	-/87.69
Capacity (kWh) $HESS_{min}/HESS_{v}$	1.11/9.55	0.49/9.84	1.80/9.85	-/11.64	5.84/22.81	5.70/24.23	6.67/24.24	-/25.05
Internal Resistance (mΩ) 50% SOC								
LIB $HESS_{min}$	91.25	547.52	273.76	7.11	14.03	14.80	16.10	3.15
SC $HESS_{min}$	1.23	2.11	3.32	-	1.44	2.11	2.71	-
LIB $HESS_{V}$	8.17	7.93	7.93	-	3.42	3.22	3.22	-
SC $HESS_{V}$	8.64	8.45	14.95	-	8.64	16.90	29.90	-

Table 6. Technical data of virtual LCO (H)ESS concept study within Gen1 and Gen3 scenarios.

Characteristic/Profile	Gen1–HEV				Gen3–WLTP			
	EDLC	**LIC_{SHC}**	**LIC_{PHC}**	**ESS**	**EDLC**	**LIC_{SHC}**	**LIC_{PHC}**	**ESS**
LIB bank (xSyP) $HESS_{min}/HESS_v$	12S7P/12S86P	12S2P/12S65P	12S1P/12S65P	-/12S125P	12S66P/12S248P	12S59P/12S272P	12S60P/12S272P	-/12S284P
SC bank (xSyP) $HESS_{min}/HESS_v$	18S6P/18S2P	13S6P/13S6P	13S8P/13S6P	-	18S5P/18S1P	13S6P/13S1P	13S9P/13S1P	-
Weight (kg) $HESS_{min}/HESS_v$	62.35/68.97	20.25/56.94	28.65/58.50	-/72.00	86.61/152.56	53.48/159.92	66.15/160.18	-/163.58
Volume (l) $HESS_{min}/HESS_v$	43.54/31.58	12.25/25.10	15.99/25.10	-/25.50	48.56/57.61	23.87/57.46	30.00/57.46	-/57.93
Capacity (kWh) $HESS_{min}/HESS_v$	0.87/8.49	0.45/7.04	1.40/7.08	-/15.44	6.48/24.50	6.38/29.43	7.10/29.43	-/33.39
Internal Resistance (mΩ) 50% SOC								
LIB $HESS_{min}$	147.23	515.33	1030	8.25	15.62	17.45	17.18	3.63
SC $HESS_{min}$	1.44	2.82	3.74	-	1.73	2.82	3.32	-
LIB $HESS_V$	11.98	15.86	15.86	-	4.15	3.78	3.79	-
SC $HESS_V$	4.32	2.82	4.98	-	8.64	16.90	29.90	-

Table 7. Technical data of virtual (H)ESS concept study within Gen1 and Gen3 scenarios versus LFP_{HP}.

Characteristic/HESS	LCO-LIC_{SHC}	LFP_{HE}-LIC_{SHC}	LFP_{HP}-LIC_{SHC}	ESS LFP_{HP}	LFP_{HP}-LIC_{SHC}	ESS LFP_{HP}
	Gen1–HEV	**Gen1–HEV**	**Gen1–HEV**	**Gen1–HEV**	**Gen3–WLTP**	**Gen3–WLTP**
LIB bank (xSyP)	12S2P	14S1P	14S2P	14S23P	14S12P	14S53P
SC bank (xSyP)	13S6P	13S8P	13S4P	-	13S4P	-
Weight (kg)	20.25	27.19	15.10	24.47	25.60	56.39
Volume (l)	12.25	16.29	8.90	11.59	13.90	26.71
Capacity (kWh)	0.45	0.49	0.41	2.90	1.43	6.36
Internal Resistance (mΩ) 50% SOC						
LIB	515.33	547.52	187.21	16.28	31.20	7.06
SC	2.82	2.11	4.22	-	4.22	-

Table 8. Target specification for 48 V mild hybrid electric vehicles in Gen1 and Gen3 application.

Characteristic	Gen1 [1]	Gen3 [2,11,18]
Maximum weight (kg)	<8	<40
Maximum power (kW)	11	25
Energy (kWh)	0.3	1–5
Energy density ($Whkg^{-1}$) *	37.5	25–125
P/E ratio *	37	25–5

* Calculated based on given weight and power values.

5. Results

5.1. Experimental Results

The measured load current I_{load} and LIB current I_{LIB} for all C2C systems under study are presented in Figure 6 along with the measured temperature of the LIB. Generally it can be seen that during discharge pulses the battery current I_{LIB} is in comparision to the charging phases tremendously reduced. The degree of current distribution between the LIB and the SC differs between the hybrid systems. As an example, it can be seen in Figure 6d that in the LCO-LIC_{PHC} system the LCO cell is barely stressed during pulse discharging and constant charging periods in which the LIC_{PHC} cell takes most of I_{load}. In comparision to that, in almost all hybrid systems using EDLC the LIB takes almost the complete load I_{load} during charging and approximately the half of the current load I_{load} during pulse discharging periods. During pulse discharging the temperature of the LIB is approx 25 °C and rises to a maximum of approx 30 °C during constant charging periods.

Energy density and power density of HESS spread for a pulse duration PD of 10 s with duty cycle D of 0.5 from 9.5 up to 55.4 $Whkg^{-1}$ and 9.7 to 65.8 Wkg^{-1} on C2C level (see Figure 7a). Highest energy and power density values are achieved by HESS existing of LFP_{HE} and LIC_{PHC} (55.4 $Whkg^{-1}$; 65.8 Wkg^{-1}). Considering LCO HESS, using LIC_{PHC} are leading to the highest e_{ESS} for LCO HESS as well.

In the comparison of LFP_{HE}-EDLC HESS on C2C to S2S level, it can be seen that power and energy density increase by more than a factor of 5. In the case of LFP_{HE}-LIC_{PHC} HESS, the factor of increasing power and energy density is approximately 1.5 and with 84.5 $Whkg^{-1}$ and 110 Wkg^{-1} highest values of energy and power density of all HESS are achieved for 10 sec pulse duration at a duty cycle of 0.5.

Changing the pulse duration PD from 10 to 2 s at a duty cycle D of 0.03, power density increases for both HESS in S2S campaign by maintaining constant energy density at the same time (see Figure 7b). Power densities at 2 s pulse duration are for LFP_{HE}-EDLC HESS 169 Wkg^{-1} and for LFP_{HE}-LIC_{PHC} HESS 194 Wkg^{-1}, whereas for LFP_{HE}-LIC_{PHC} HESS the difference in power density between 5 s and 2 s pulse duration is only approximately 10 Wkg^{-1}. Compared to 48 V LFP ESS, it is an increase in power density up to a factor of 1.9 by a reduction of energy density up to 14%. Maximum temperature, which arised within the LFP_{HE} 48 V system has been 34.8 °C at the test pulse test procedure with 10 s PD and 0.5 D regime.

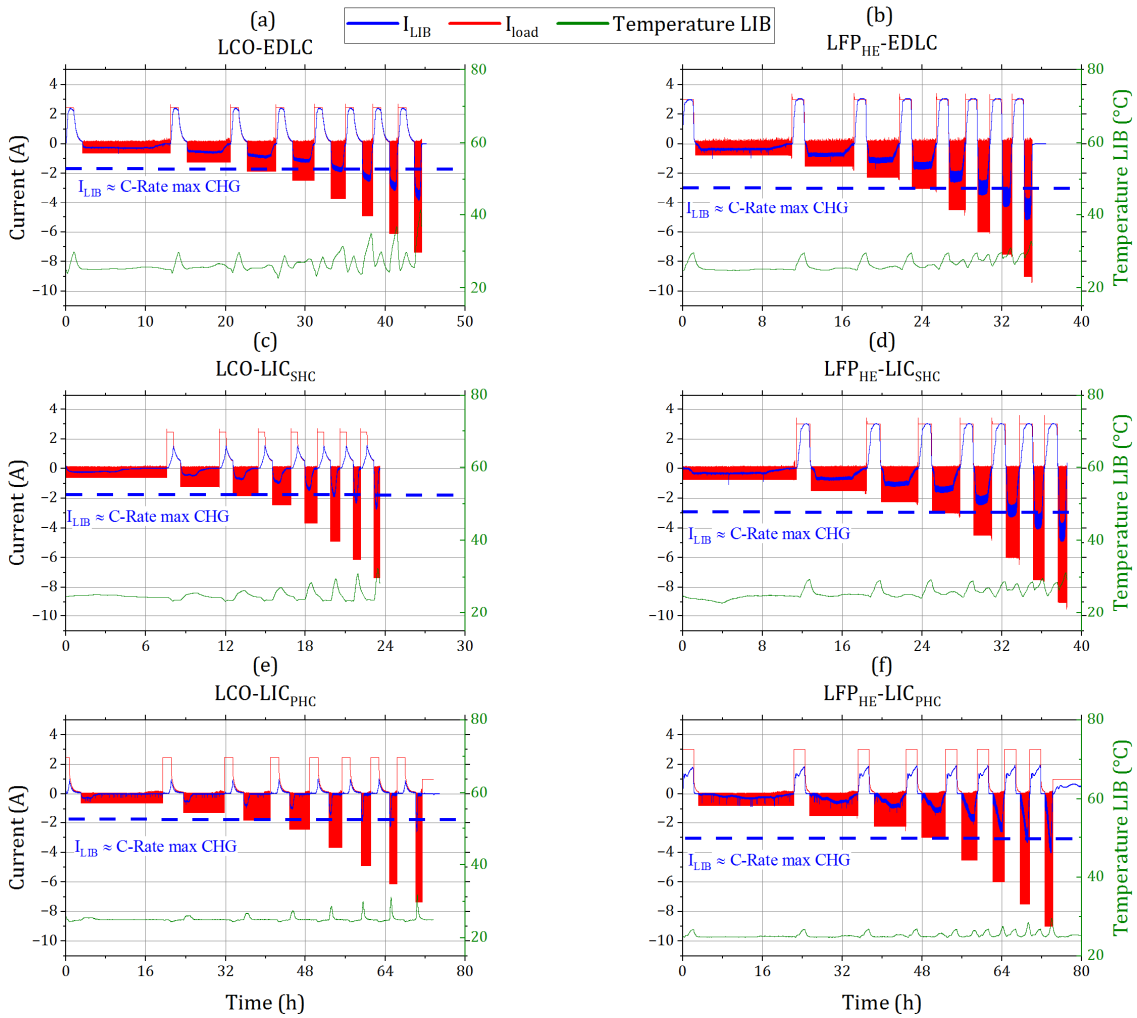

Figure 6. Load profile I_{load}, LIB current I_{LIB} and recorded LIB temperature during energy and power density characterization for hybrid systems on C2C level. The load of the supercapacitor results in the difference of I_{LIB} and the load I_{load}. For the power density, only I_{LIB} values which are not exceeding the current equivalent of the max C-Rate in higher than in charge (CHG) direction are considered.

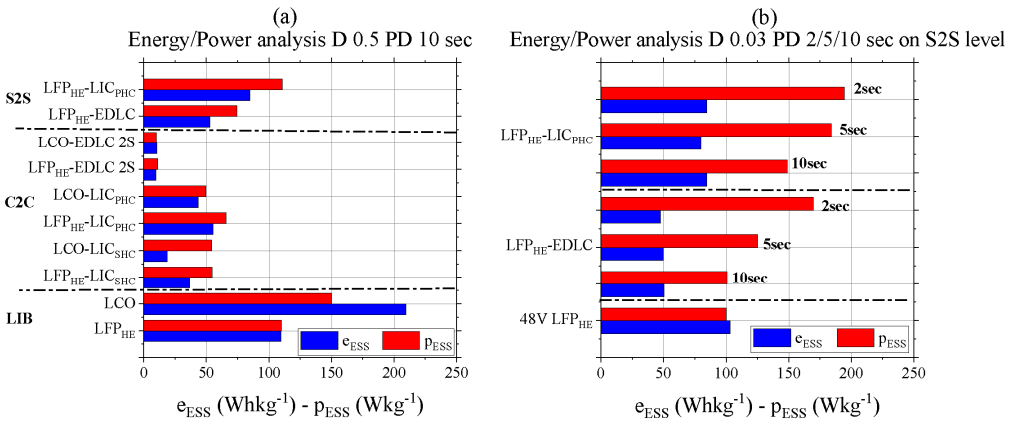

Figure 7. (**a**) Energy and power density analysis for C2C and S2S campaign at PD 10 s and D of 0.5; (**b**) energy and power density analysis for S2S campaign at constant D of 0.03 and load pulses of 2, 5, and 10 s PD.

5.2. Model Validation

Exemplary profiles of the validation campaign for the cell and the system model on a C2C and S2S level are given in Figure 8. The average overall accuracy of the model for each campaign, and the number of considered errors is presented in Table 9. Voltage error increases from 1.95% for the cell model CM up to 3.44% for S2S analysis. The model error of the electrical current shows a similar trend. Herein, the mean error increases from C2C analysis to S2S analysis from 6.33% to 7.42%.

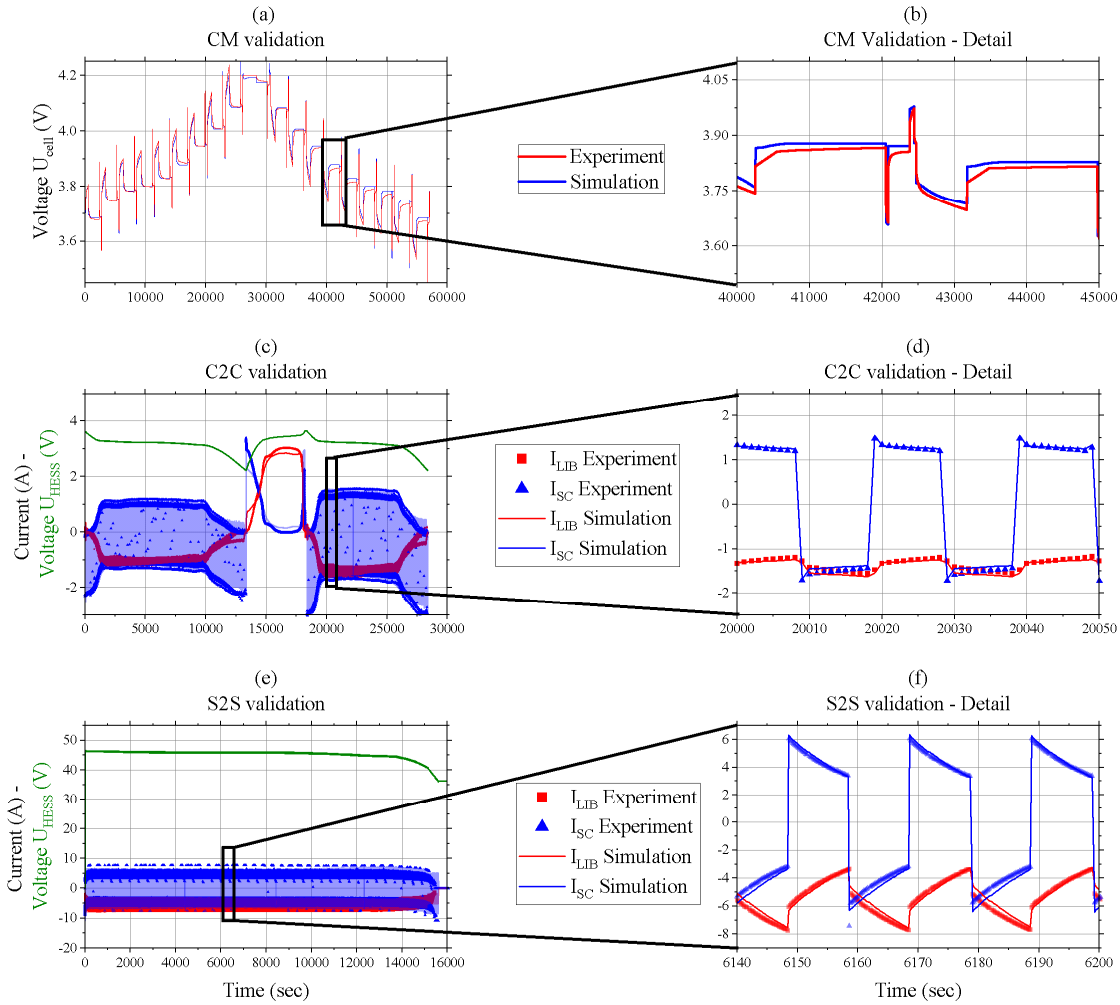

Figure 8. Measured and simulated currents and terminal voltage profiles; (**a**,**b**) measured and simulated voltage behavior of lithium-ion cobalt oxide (LCO); (**c**,**d**) modeled and measured current profile of LFP_{HE}-LIC_{SHC} HESS of C2C campaign along with system voltage U_{HESS}; (**e**,**f**) modeled and measured current profile of LFP_{HE}-EDLC hybrid of S2S campaign along with measured terminal voltage U_{HESS}.

Table 9. Average overall model accuracy for cell model (CM), cell to cell analysis (C2C), and system to system analysis (S2S) analysis given as normalized-root-mean-square error (NRMSE).

Campaign	Number of Errors	Voltage (%)	Current (%)
CM	6	1.95	-
C2C	12	2.94	6.33
S2S	4	3.44	7.42

5.3. Results of the Virtual Concept Study

The analysis of the performance index Θ within the Gen1 scenario is presented in Figure 9, whereas Figure 9a,b is presenting LFP_{HE} and LCO hybrid systems with minimized system dimensions ($HESS_{min}$), and Figure 9c,d is showing the results of the performance index for systems that have approximately the same volume ($HESS_v$) as their competitor battery-only system. It is shown in Figure 9a,b that by using LIC technology a reduction of up to 60% in weight and volume is possible for both LIB technologies under study. However, the single cell stress within the LIB bank is up to 60% higher than in the competitive battery-only system. An exception is hybrid systems using the parallel LIC technology. Herein, approximately same stress levels are achieved as in the battery-only system.

The hybrid systems using LCO as LIB bank are slightly more stressed than hybrid systems using LFP_{HE}. Using the classical EDLC technology for a hybrid system leads to a reduction in weight but the required volume is up 70% higher (in case of LCO-EDLC) than for its counterpart. Increasing the hybrid system to the approximately same volume as its battery-only counterpart leads generally to a reduction of the single cell stress within the LIB bank.

The highest reductions are achieved for LCO-LIC_{SHC} and LCO-LIC_{PHC} hybrid systems with more than 30% in charge throughput Q_{TP} and current stress I_{RMS}. In the case of the LFP_{HE} hybrid systems, using the serial or even the parallel LIC, a reduction of up to 20% is possible. A hybrid system made up of EDLCs with approximately the same volume of its battery counterpart and without overstraining the LIB-bank is only possible by using LFP_{HE}.

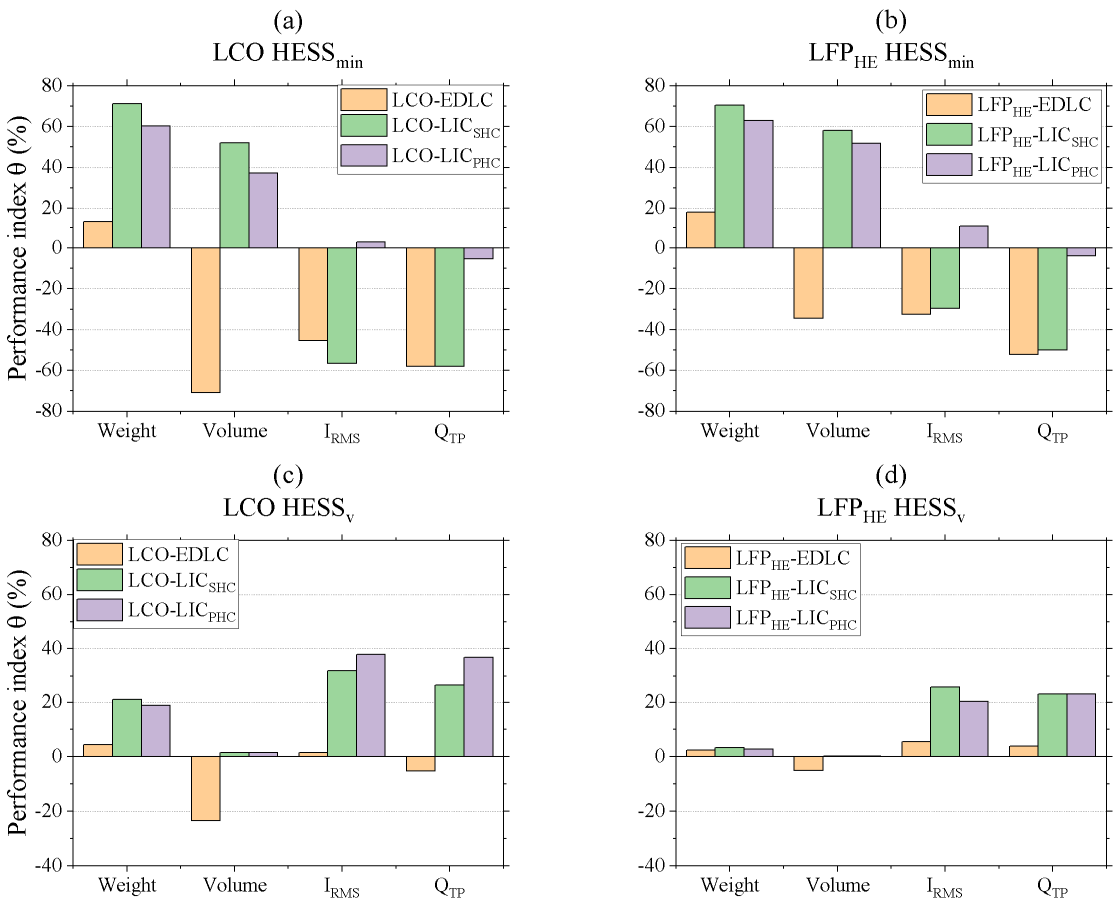

Figure 9. Performance index comparison of hybrid systems using different LB and SC technologies and design criteria for Gen1 applications versus battery-only systems using same LIB technology; (**a**,**b**) performance index of lightest hybrid systems; (**c**,**d**) performance index of volume equivalent hybrid systems.

Figure 10 presents the results of the Gen3 scenario analysis. Moreover, here a tremendous reduction of the system dimensions in weight and volume can be achieved compared to the battery-only system. In Figure 10a,b it can be seen that LFP_{HE} hybrid systems and LCO hybrid systems achieve a weight and volume reduction from 20% up to 60% depending on the used supercapacitor technology.

Moreover, here the small system size leads to an increase in single cell stress compared to the battery-only system. The current is for all hybrid systems between 30% and 80% higher than their battery-only counterpart. The charge throughput Q_{TP} within the LCO hybrid systems is 50% to 70% higher than in the LCO battery systems and is quite similar for the LCO-EDLC and LCO-LIC_{SHC} hybrid. Within the LFP_{HE} hybrid systems, the single cells get approximately up to more than 100% stressed than in the LFP_{HE} battery system.

Moreover, the Gen3 scenario hybrid systems with approximately the same volume as their battery-only counterpart tend to a reduction of charge throughput Q_{TP} and root mean square current I_{RMS}. In the case of the LCO hybrids, the single cells within the LCO bank are exposed to the same charge throughput as in the LCO battery system. Simultaneously the root mean square current I_{RMS} is reduced up to 6% using serial or even parallel LIC. In case of using EDLC, the root mean square current is for a cell within the LCO bank 4% higher than in the LCO battery system.

The LFP_{HE} hybrid systems tend to similar results as LCO hybrid systems within this scenario. The only differences are that besides the root mean square current, also the charge throughput Q_{TP} is reduced up to 4% by using LIC. Using EDLC leads to an increased charge throughput of 2%.

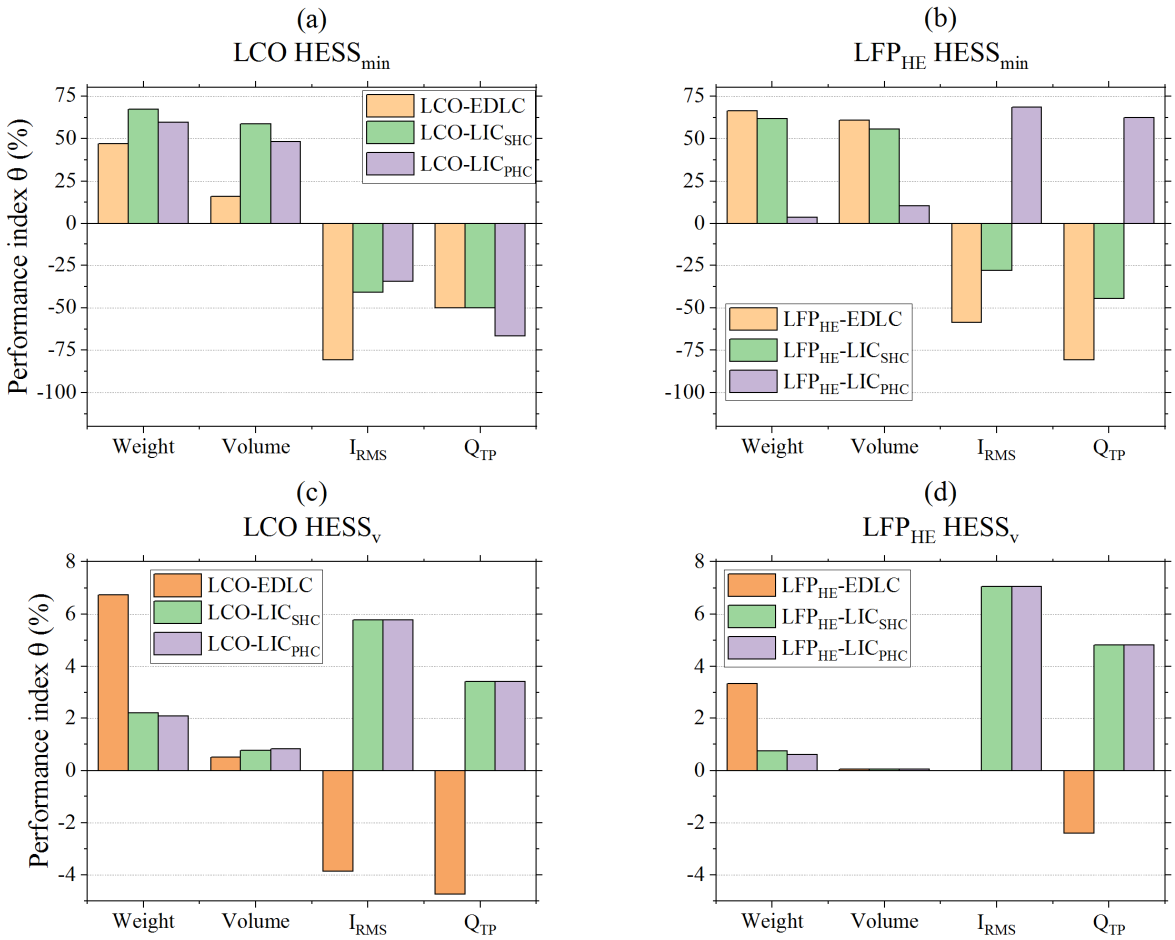

Figure 10. Performance index comparison of hybrid systems using different LIB and SC technologies and design criteria for Gen3 applications versus battery-only systems with same LIB technology; (**a**,**b**) performance index of lightest hybrid systems; (**c**,**d**) performance index of volume equivalent hybrid systems.

The results of the comparison of hybrid systems using high energy cells versus high power systems within Gen1 applications are presented in Figure 11a. Generally, the single cell stress is in both hybrid systems reduced up to 60% less than in the competitive LFP_{HP} system, but only the $LCO\text{-}LIC_{SHC}$ hybrid meets the requirements to not exceed the system dimension of the LFP_{HP} system.

Figure 11a shows the performance index of a $LFP_{HP}\text{-}LIC_{SHC}$ hybrid system within Gen1 and Gen3 applications versus a LFP_{HP} system. Moreover, here it can be seen that even for Gen1 and Gen3, a reduction of the system dimension is possible. Depending on the scenario, weight and volume are reduced between 20% and 50%. In Gen1, the single cell stress is reduced up to 20% whereas for Gen3 scenario the single battery cell is up to 50% more strained than in the competitive LFP_{HP} system.

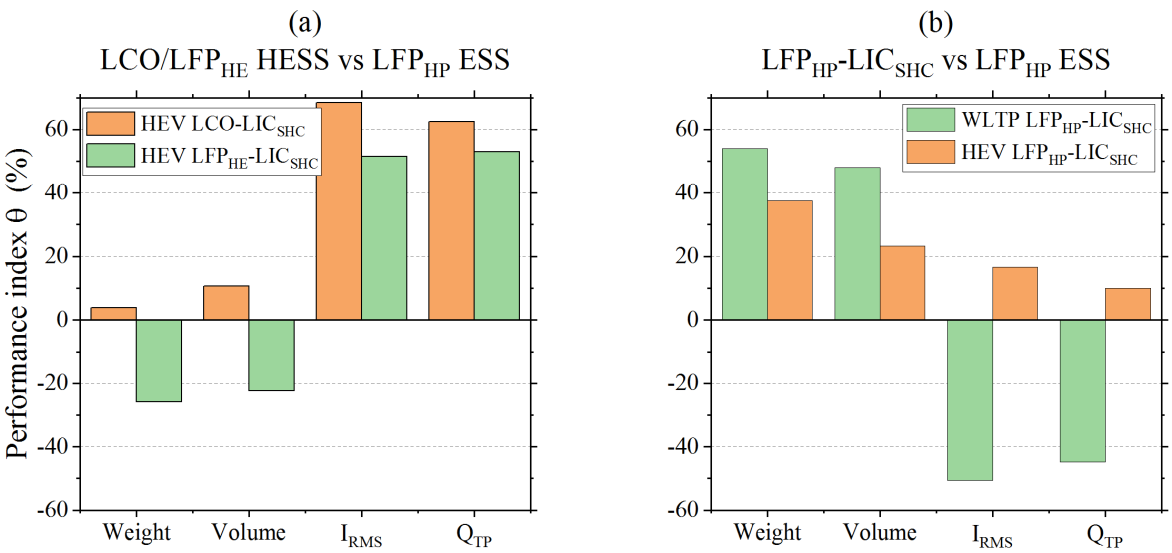

Figure 11. (**a**) Performance index for hybrid systems using high energy cells versus battery-only systems with LFP_{HP} high power cells within Gen1 application; (**b**) comparison of hybrid systems using $LFP_{HP}\text{-}LIC_{SHC}$ setup versus battery-only LFP_{HP} system within Gen1 and Gen3 application.

Finally, the hybrid systems and the battery-only systems shall be classified concerning their gravimetric energy density P/E ratio. The results are given in Figure 12, which also highlights the target areas for Gen1 and Gen3 values.

At first sight, hybrid systems, which are designed to achieve the same volume ($HESS_v$) as their battery-only counterpart, diverge to areas where their battery-only counterpart is located. Those systems achieve approximately the same P/E ratio as the LIB technology that is used, but simultaneously, a lack in energy density compared to its single LIB-ion technology occurs. In case of using LCO as LIB bank, the energy density is up to 40% reduced compared to the corresponding LCO battery-only system. Considering LFP_{HE} battery-only and HESS systems, energy density is less than 10% reduced.

However, minimized hybrid systems ($HESS_{min}$) are lifting the P/E ratio of the single LIB technology into the desired target areas. The high energy cells of this study LFP_{HE} and LCO are able to fulfill partially Gen1 conditions concerning P/E ratio and energy density by a passive hybridization with a serial LIC. Furthermore, it should be emphasized that hybrid systems using $LFP_{HP}\text{-}LIC_{SHC}$ fulfill the target areas of Gen1 and Gen3 applications.

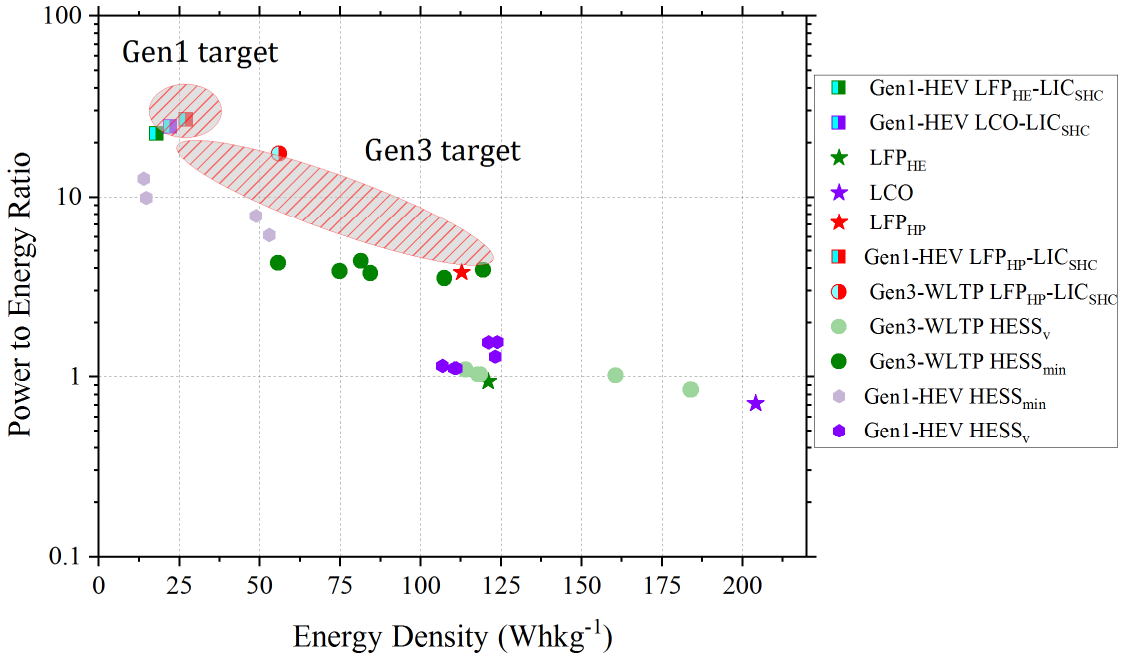

Figure 12. Power to energy ratio and corresponding to technical data of hybrid and battery-only systems of Tables 5–7 as well as target areas for Gen1 and Gen3 applications according to Table 8.

6. Discussion

Experimental and model-based investigations have shown that passive HESS can be a suitable approach for present and future generations of MHEV. However, several factors that influence the performance of a HESS have to be considered. The experimental campaign highlighted the influence of the HESS setup on its performance. Besides the influence of technology matching on cell level, improvements in power and energy density of the same composition up to a factor 5 on system level are possible. Furthermore, the characteristic of the pulse load profile influences the performance of a HESS. Shorter pulse lengths are leading to higher power densities. In general, a hybridization of LIB with LIC technologies leads to better performances than the other HESS. In comparison to HESS using EDLC, the energy density is improved by similar voltage levels of LIB and LIC combined with an improved energy density of LIC over EDLC. Power density is improved, hence LIC are able, due to their higher amount of energy density, to get charged/discharged for a longer period of time until the LIB has to take most part of the load. With this, higher current loads are possible without overstraining the LIB.

Within the experiment the best performance is shown by the 48 V LFP_{HE}-LIC_{PHC} HESS. In comparison to the LFP battery-only system, an increase in power density up to a factor of 1.9 can be achieved. This comes with the drawback of a loss in energy density by 14%.

The model-based campaign has proven that the used approach of a universal model for the different technologies is quite accurate on cell and system level. It is clear that the model error increases from cell to system level as the number of external factors increase due to the increased complexity from ESS to a single cell. Still, the maximum error of 7% within eight different HESS setups using five different technologies is quite satisfying when taken the high dynamics in current and voltage into account that exist within a passive HESS under pulse current load. Moreover, most model errors arise in low SOC area (<10%) in which high voltage dynamics occur.

The virtual concept study shows for both scenarios that the HESS approach is quite suitable for MHEV applications. The system dimensions can be minimized up to 60% and even HESS using high-energy cells can compete with high power systems in Gen1 applications. Nevertheless, the system layout and technology matching have an extreme influence on the P/E ratio and energy density.

A hybridization can shift P/E ratio and energy density values into areas which are suitable for desired applications which cannot be met by a technology on its own.

It has been shown that HESS with approximately the same dimensions as its LIB counterpart have also a quite similar P/E and energy density characteristics but less battery stress, whereas minimized HESS have to endure higher battery stress, which is still within data sheet limitations. Impacts on aging shall be analyzed in future studies along with standardized layout criteria for optimal HESS design.

7. Conclusions

In this work, passive hybrid energy storage systems were investigated on cell and system level for different lithium-ion and supercapacitor technologies within pulse load applications. The hybrid energy storage system performance was influenced by the technology match and also by the characteristics of the pulse profile. In addition, a universal model and its parameterization for lithium-ion and supercapacitor technologies were presented and its validity on cell and system modeling was proven. A virtual concept study for two generations of mild hybrid electric vehicles was shown. In general, passive hybrid energy storage systems show a better power to energy ratio along with less necessary weight and volume than competitive battery-only energy storage systems, especially in high dynamic profiles. For pure electric driving scenarios, passive hybrid energy storage systems still show a better power to energy ratio, but lithium-ion batteries have to endure a higher charge throughput than their competitive battery-only energy storage systems. Impacts on aging behavior shall be part of further studies as well as a proposal of a design process for hybrid energy storage systems.

Author Contributions: Conceptualization, methodology, software, formal analysis, investigation, writing—original draft preparation, T.G.; writing—review and editing, supervision, M.D.

Funding: This research received no external funding.

Acknowledgments: The authors thank Anna Smith and her research group from Institute for Applied Materials at Karlsruhe Institute of Technology for supplying cell data and also the necessary test environment and equipment. We also would like to thank Manuel Baena and Alexis Kalk from Institute of Electrical Engineering at Karlsruhe Institute of Technology for their support in developing and assembling the 48 V prototypes and their BMS.

Conflicts of Interest: The authors declare no conflict of interest.

References

1. The Idaho National Laboratory. U.S. Department of Energy Vehicle Technologies Program Battery Test Manual for 48 Volt Mild Hybrid Electric Vehicles. 2017. Available online: https://inldigitallibrary.inl.gov/sites/sti/sti/7364006.pdf (accessed on 5 June 2019).
2. Degenhart, E. Powertrain Review Powertrain Strategy 2020 +. Available online: https://www.continental-corporation.com/resource/blob/33902/50729be3c974864761524b7de1a8f625/2017-04-25-presentatione-powertrain-strategy-data.pdf (accessed on 10 October 2018).
3. Chuan, Y.; Mi, C.; Zhang, M. Comparative study of a passive hybrid energy storage system using lithium ion battery and ultracapacitor. *World Electr. Veh. J.* **2012**, *5*, 83–90. [CrossRef]
4. Naoi, K.; Ishimoto, S.; Miyamoto, J.; Naoi, W. Second generation 'nanohybrid supercapacitor': Evolution of capacitive energy storage devices. *Energy Environ. Sci.* **2012**, *5*, 9363–9373. [CrossRef]
5. Dubal, D.P.; Ayyad, O.; Ruiz, V.; Gómez-Romero, P. Hybrid energy storage: The merging of battery and supercapacitor chemistries. *Chem. Soc. Rev.* **2015**, *44*, 1777–1790. [CrossRef] [PubMed]
6. Cericola, D.; Kötz, R. Hybridization of rechargeable batteries and electrochemical capacitors: Principles and limits. *Electrochim. Acta* **2012**, *72*, 1–17. [CrossRef]
7. Cericola, D.; Ruch, P.W.; Kötz, R.; Novák, P.; Wokaun, A. Simulation of a supercapacitor/Li-ion battery hybrid for pulsed applications. *J. Power Sources* **2010**, *195*, 2731–2736. [CrossRef]
8. Kuperman, A.; Aharon, I. Battery-ultracapacitor hybrids for pulsed current loads: A review. *Renew. Sustain. Energy Rev.* **2011**, *15*, 981–992. [CrossRef]
9. Dougal, R.A.; Liu, S.; White, R.E. Power and life extension of battery-ultracapacitor hybrids. *IEEE Trans. Components Packag. Technol.* **2002**, *25*, 120–131. [CrossRef]

10. Holland, C.E.; Weidner, J.W.; Dougal, R.A.; White, R.E. Experimental characterization of hybrid power systems under pulse current loads. *J. Power Sources* **2002**, *109*, 32–37. [CrossRef]
11. Warner, J. *The Handbook of Lithium-Ion Battery Pack Design*; Elsevier Science: Amsterdam, The Netherlands, 2015.
12. Budde-Meiwes, H.; Drillkens, J.; Lunz, B.; Muennix, J.; Rothgang, S.; Kowal, J.; Sauer, D.U. A review of current automotive battery technology and future prospects. *Proc. Inst. Mech. Eng. Part D J. Automob. Eng.* **2013**, *227*, 761–776. [CrossRef]
13. Mousavi, G.S.M.; Nikdel, M. Various battery models for various simulation studies and applications. *Renew. Sustain. Energy Rev.* **2014**, *32*, 477–485. [CrossRef]
14. Seaman, A.; Dao, T.S.; McPhee, J. A survey of mathematics-based equivalent-circuit and electrochemical battery models for hybrid and electric vehicle simulation. *J. Power Sources* **2014**, *256*, 410–423. [CrossRef]
15. Zhang, L.; Wang, Z.; Hu, X.; Sun, F.; Dorrell, D.G. A comparative study of equivalent circuit models of ultracapacitors for electric vehicles. *J. Power Sources* **2015**, *274*, 899–906. [CrossRef]
16. Schweiger, H.-G.; Obeidi, O.; Komesker, O.; Raschke, A.; Schiemann, M.; Zehner, C.; Gehnen, M.; Keller, M.; Birke, P. Comparison of several methods for determining the internal resistance of lithium ion cells. *Sensors (Basel)* **2010**, *10*, 5604–5625. [CrossRef] [PubMed]
17. Dubarry, M.; Vuillaume, N.; Liaw, B.Y. From single cell model to battery pack simulation for Li-ion batteries. *J. Power Sources* **2009**, *186*, 500–507. [CrossRef]
18. Wu, X.; Freese, D.; Cabrera, A.; Kitch, W.A. Electric vehicles energy consumption measurement and estimation. *Transp. Res. Part. D Transp. Environ.* **2015**, *34*, 52–67. [CrossRef]